Compression-induced buckling of a semiflexible filament in two and three dimensions Θ

Ananya Mondal ; Greg Morrison ■



J. Chem. Phys. 157, 104903 (2022) https://doi.org/10.1063/5.0104910





CrossMark

Downloaded from http://pubs.aip.org/aip/jcp/article-pdf/doi/10.1063/5.0104910/16551736/104903_1_online.pdf

Articles You May Be Interested In

Semiflexible Polymers and Filaments: From Variational Problems to Fluctuations

AIP Conference Proceedings (April 2008)

Compression induced phase transition of nematic brush: A mean-field theory study

J. Chem. Phys. (November 2015)

Three-dimensional dynamic Monte Carlo simulations of elastic actin-like ratchets

J. Chem. Phys. (November 2005)





Compression-induced buckling of a semiflexible filament in two and three dimensions

Cite as: J. Chem. Phys. 157, 104903 (2022); doi: 10.1063/5.0104910

Submitted: 21 June 2022 · Accepted: 21 August 2022 ·

Published Online: 14 September 2022







Ananya Mondal^{1,2,a)} and Greg Morrison^{1,2,b)}





AFFILIATIONS

- Department of Physics, University of Houston, Houston, Texas 77204, USA
- ²The Center for Theoretical Biological Physics, Rice University, Houston, Texas 77005, USA
- a) amondal 2@uh.edu
- b) Author to whom correspondence should be addressed: gcmorrison@uh.edu

ABSTRACT

The ability of biomolecules to exert forces on their surroundings or resist compression from the environment is essential in a variety of biologically relevant contexts. For filaments in the low-temperature limit and under a constant compressive force, Euler buckling theory predicts a sudden transition from a compressed state to a bent state in these slender rods. In this paper, we use a mean-field theory to show that if a semiflexible chain is compressed at a finite temperature with a fixed end-to-end distance (permitting fluctuations in the compressive forces), it exhibits a continuous phase transition to a buckled state at a critical level of compression. We determine a quantitatively accurate prediction of the transverse position distribution function of the midpoint of the chain that indicates this transition. We find that the mean compressive forces are non-monotonic as the extension of the filament varies, consistent with the observation that strongly buckled filaments are less able to bear an external load. We also find that for the fixed extension (isometric) ensemble, the buckling transition does not coincide with the local minimum of the mean force (in contrast to Euler buckling). We also show that the theory is highly sensitive to fluctuations in length in two dimensions and the buckling transition can still be accurately recovered by accounting for those fluctuations. These predictions may be useful in understanding the behavior of filamentous biomolecules compressed by fluctuating forces, relevant in a variety of biological

Published under an exclusive license by AIP Publishing. https://doi.org/10.1063/5.0104910

I. INTRODUCTION

Buckling is defined as the process by which a slender column bends laterally under an axial compressive load. At the cellular level, buckling instabilities have been observed 1-6 to occur in biological systems as well with cytoskeletal filaments, such as F-actin, which buckle during cell deformation. The ability of a single or bundled cytoskeletal filaments to exert forces, support an external load, or deform membranes is essential for many biological processes,⁷ and it is important to relate the mechanical properties of the filaments to their ability to perform these functions. Deformation forces resulting from cell shape changes can also lead to internal re-organization of cross-linked actin bundles¹⁵⁻¹⁹ and can induce buckling in some cases. The ends of actin filaments inside a cell can be mechanically coupled to other biomolecules forming the cytoskeletal network,²⁰⁻ and these attachment conditions can generate contractile forces inducing buckling. Other more complex cases of buckling inside a cell arise from actomyosin

contractility^{27–31} involving ATP-dependent compression by myosin-motors or even axial compression on the actin bundles by cell membrane tension. 32-34 Actomyosin contractility can also lead to many interesting phenomena such as helical buckling^{35–37} or development of sharp kinks^{38–45} that eventually cause sharply bent filaments to sever.

In addition to experimental studies of buckling in vivo, numerous *in vitro* studies have probed the responses of semiflexible biomolecules to compressive forces using single-molecule force experiments for single filaments, 23,46-51 cross-linked bundles, 52 and networks. 17,44 Cross-linked actin networks exhibit strain-stiffening^{55–58} a characteristic property of semiflexible polymers that show greater resistance to elongation the more they are stretched. At high strains, part of the network also experiences compression, and actin filaments tend to buckle⁵⁹ leading to severing. As a model to explore the role of deformation forces on buckling in the actomyosin cell cortex, artificially made giant unilamellar vesicles (GUVs) are used^{5,6,44,60,61} to mimic the effects of forces exerted by cell membrane on the reconstituted cytoskeletal network. Microfluidic experiments on semiflexible actin filaments in extensional flows have also shown a stretch-coil transition, with a competition between elasticity and tension causing the actin filaments to buckle. Buckling has also been reported in ring polymers under spherical confinement, which are found in many naturally occurring systems, such as viral capsids or circular DNA in bacteria. These non-equilibrium processes may play important roles in many biologically relevant systems, but even the buckling of a single filament in the presence of thermal fluctuations remains poorly understood at equilibrium.

On a macroscopic scale, the buckling of columns and elastic rods has been studied for centuries. According to the Euler buckling theory,⁷² an elastic rod buckles when the compressive force exceeds a critical value in a sharp transition in the absence of thermal fluctuations. On a microscopic level, the buckling of single biomolecules at finite temperatures has been observed experimentally^{6,23,44} and theoretically.^{73,74} The buckling transition depends strongly on the mechanical properties of the filament. For example, F-actin has a persistence length (l_p) that varies between 10 and 20 μ m^{11,75} and the typical length (L) of the filaments found in a filopodium is of the order of 1–10 μ m. At finite temperatures, the filament fluctuates, and the local orientation of the filament varies on the length scale of the persistence length. The mechanical properties of these thermally fluctuating F-actin filaments dictate a cell's response to environmental cues, and therefore, a good understanding of the buckling process in the presence of thermal fluctuations is essential.

To model the buckling process in filamentous biomolecules, the responses to compressive forces are studied in two different ensembles:76-79 isometric and isotensional. These ensembles are equivalent to the Helmholtz (fixed volume) and Gibbs (fixed pressure) ensembles of classical statistical mechanics, respectively. An isometric ensemble is obtained by tethering the endpoints of the polymer, where the applied force fluctuates. In the isotensional ensemble, the fixed force stretches or compresses the chain and the fluctuating end-to-end distance of a polymer is measured. Classical Euler buckling is in the isotensional ensemble, with a constant compressive force, but in the absence of thermal fluctuations. The equivalence between these two ensembles has been explicitly demonstrated 77,78 for an unconfined polymer under an applied tension, but differences between the ensembles have been found in the thermodynamic limit in some cases, including confined polymers under tension.⁷⁹ For finite length chains, the isometric ensemble will have a fluctuating force at the endpoints, and equivalence between the isometric and isotensional ensembles can only be realized in the $L \to \infty$ limit.⁷⁸ For finite length chains, we expect differences between these two ensembles, including the critical compression force (in the isotensional ensemble) or mean compression force (in the isometric ensemble) at which buckling occurs. In this paper, we will focus primarily on the statistics of isometric systems. It is important to note that, while isotensional experiments are readily performed using optical tweezers, the most appropriate ensemble in vivo may depend on the system of interest. For example, the ends of actin filaments inside of the cell can be found trapped between other biomolecules. 20-22,80 Stretching or compression of these filaments may be primarily due to the endpoint constraints, rather than a constant applied force. In addition to the pinning of the endpoints of

the chain, many authors \$1,82 have studied the effect of constraints on the orientation of the bonds at the endpoints as well. These include "clamped" (both bonds constrained to be aligned with the compressive force), "cantilevered" (one bond constrained to be aligned with the force axis), and "free" (no constraint on the endpoint bonds). The critical compression at which buckling occurs will depend on the specific endpoint ensemble chosen, but buckling is expected to occur in all three ensembles at some compression. In this paper, we focus only on the free bond ensemble but discuss the application of the other endpoint constraints in Sec. IV.

The wormlike chain (WLC) theory⁸³ is widely used to model semiflexible polymers. The WLC is a continuum theory for slender filaments, incorporating both inextensibility and a length scale, l_p , called the persistence length. Deriving statistical quantities from the WLC model exactly involves solving the path integral of a quantum particle^{84,85} on the surface of a sphere. A substantial number of numerical studies have explored the process of buckling in single,⁴⁸ bundled, 86,87 and confined wormlike chains. While statistical averages can usually be determined numerically using wellestablished techniques for solving the Schrödinger equation with a nonlinear potential, it is often the case that analytically tractable results are not easily determined. 73,81,82,90-92 To overcome this limitation, approximate methods, such as mean-field (MF) theories for wormlike chains, 74,93-98 provide analytically tractable quantitative predictions for a variety of equilibrium statistics that can be more easily applied to experimental data. Previously, the authors in Ref. 99 have taken a mean-field theoretical approach to model filament buckling and they have found a weakly first-order transition between unbuckled and buckled states in the isotensional ensemble. Despite this theoretical effort, many details of the buckling of a filament, such as the end-to-end distribution functions, remain poorly predicted on a quantitative level. As a result, more work is required to fill the gap in developing a theory for the buckling process in wormlike chains that will have both experimentally accessible predictions as well as biological

In this paper, we use an analytically tractable mean-field theory combined with Monte Carlo simulations to determine the statistics of wormlike chains constrained to have fixed end-to-end distance in two and three dimensions. In Sec. II, we describe the mathematical and computational models. In Sec. III B, we derive the end-to-end distribution for semiflexible chains, recovering a well-known result¹⁰⁰ in three dimensions but finding poor agreement with simulations in two dimensions. We show, in Sec. III C, that the distributions can be brought into agreement with simulations by modifying a parameter in the mean-field approximation and find that the distribution of the transverse position of the midpoint of a chain can be accurately predicted using that modification in Sec. III D. We find that the distribution transitions from unimodal to bimodal (indicating a continuous phase transition) and that the mean compressive force is nonmonotonic but that the locations of local minima in the force do not coincide with the buckling transition. Finally, in Sec. III E, we show that the distribution functions predicted in Sec. III D are highly sensitive to small fluctuations in length and the theory can be modified to qualitatively reproduce the distribution of transverse positions. We conclude with a summary of the applicability and limitations of the

II. METHODS

A. Theory

The wormlike chain model has been used to describe $^{84,101-103}$ the statistics and dynamics of a wide range of biomolecules. This continuum model incorporates two features relevant for a variety of polymers: inextensibility (fixed length L) and a resistance to bending through the Hamiltonian,

$$\beta H_{wlc} = \frac{l_p}{2} \int_0^L ds (\partial_s \hat{\mathbf{u}})^2, \tag{1}$$

where **r** is the position on the polymer, $\hat{\mathbf{u}} = |\partial \mathbf{r}/\partial s|$ is the unit vector describing the local direction of the polymer, and $\partial/\partial s$ indicates the derivative with respect to the arc-length s. The imposition of an inextensibility constraint makes the WLC model difficult to deal with analytically in all but the simplest cases, and many observables must typically be evaluated numerically. ^{73,90,91} In many cases, ^{93–95,99} analytic progress can be made by relaxing the rigid constraints of inextensibility by constraining the average length of the polymer using a Lagrange multiplier [commonly referred to as a Mean-Field (MF) model]. For an unconstrained WLC, an often used MF Hamiltonian is

$$H_0[\mathbf{u}(s)] = \delta(\mathbf{u}_0^2 + \mathbf{u}_L^2) + \frac{l_0}{2} \int_0^L ds \dot{\mathbf{u}}^2 + \lambda \int_0^L ds \mathbf{u}^2,$$
 (2)

where l_0 is a "mean-field persistence length" $(l_0 \neq l_p)$ for the unconstrained WLC, λ is a resistance to stretching along the backbone of the chain, and $\mathbf{u} = \dot{\mathbf{r}}$ is the local stretching of the chain in the continuum limit. Note that Eq. (2) does not impose any constraints on the direction of the bonds at the endpoints (only on the length of the bonds at the endpoints through the Lagrange multiplier δ). This model, thus, corresponds to a free endpoint ensemble, as opposed to clamped or cantilevered ensembles (discussed further in the conclusions). For the true WLC, the inextensibility constraint is $|\mathbf{u}(s)| = 1$. The MF approach chooses the parameters λ and δ such that inextensibility is imposed on average, with $\langle \int_0^L ds \mathbf{u}^2 \rangle_0 = L$ and $\langle {\bf u}_0^2+{\bf u}_L^2\rangle_0$ = 1 (with $\langle\cdots\rangle_0$ being a statistical average using the MF Hamiltonian in 2). The Lagrange multiplier λ constrains the length of the chain, while the Lagrange multiplier δ accounts for the excess fluctuations at the endpoints of the chain.⁹³ endpoint fluctuation terms may appear unimportant for long chains, but we will see that deriving an accurate end-to-end distance distribution function requires δ to be included in the theory (discussed further in Sec. III B). It is convenient to define the free energy for a wormlike filament as $\mathcal{F}_0 = -\log[\int \mathcal{D}[\mathbf{u}(s)]e^{-\beta H_0}] + \lambda L + 2\delta$, with the constraints imposed through $\partial \mathcal{F}_0/\partial \lambda = \partial \mathcal{F}_0/\partial \delta = 0$. The MF Hamiltonian is quadratic, making the calculation of a variety of equilibrium averages straightforward (as discussed in more detail in Sec. III A).

B. Simulation methodology

We simulate a coarse-grained bead-spring chain (as shown in Figs. 1) consisting of N = 100 beads with positions indexed as \mathbf{r}_i and (N-1) bonds with normalized bond vectors given by $\hat{\mathbf{u}}_i = (\mathbf{r}_{i+1} - \mathbf{r}_i)/|\mathbf{r}_{i+1} - \mathbf{r}_i|$. The chain length is given by L = (N-1)a, where a is

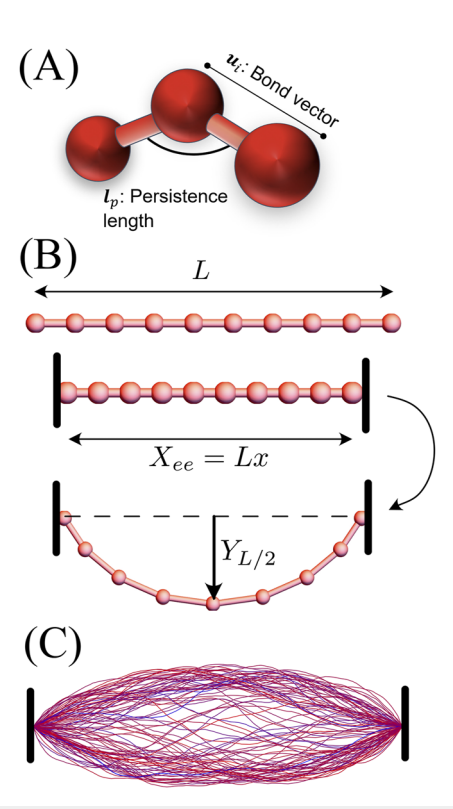


FIG. 1. Schematic diagram of the WLC model and the buckling process in our simulations. (a) The bending and stretching contributions to the energy in the simulations. (b) The initialization of the simulation: a chain of length L is compressed uniformly along the backbone to $X_{\rm ee}=0.99L$ and allowed to equilibrate as schematically diagrammed. The equilibrated configurations from x=0.99 are used as the initial conditions for x=0.98 after each bond is uniformly compressed by 1%, and the process is repeated. (c) A sample of 100 equilibrated configurations for the two-dimensional simulation with x=0.94. Configurations are colored based on their total bending energy, with red indicating greater energy. The low density in the center indicates that the system has buckled: the most probable configurations have a nonzero value of $Y_{L/2}=yL$.

the bond length. The Hamiltonian for the discretized WLC consists of two energetic contributions: the bending energy and the stretching energy of the bead-spring chain. In our simulations, the bending energy is $U_{\rm bend} = \kappa \sum_i (1 - \hat{\bf u}_i \cdot \hat{\bf u}_{i+1})$. To coarse-grain the system, we have used the persistence length, $^{104} \ l_p/a = (\kappa - 1 + \kappa \coth \kappa)/2(\kappa + 1 - \kappa \coth \kappa)$, with κ as the bending stiffness parameter. For a stiff chain, κ is large $(\kappa \to \infty)$ and so the relation reduces to $l_p/a \approx \kappa - 1/2 + O(e^{-2\kappa})$. We mapped our coarse-grained simulations onto the typical parameters for actin filaments, with persistence length being $l_p = 17 \ \mu \text{m.}^{105}$ In most of our simulations, we chose a bending stiffness of $\kappa = 99.5k_BT$ so that $l_p \approx L$. These parameters give a length of approximately $a \approx 172$ nm between the monomers. The stretching energy of the harmonic springs connecting the beads is $U_s = (\kappa_s/2)\sum_i (|{\bf u}_i| - a)^2$, where $|{\bf u}_i| = |{\bf r}_{i+1} - {\bf r}_i|/a$ is the dimensionless bond length and $\kappa_s a^2 = 490k_BT$ is the stretching stiffness used in our simulations.

We first perform Monte-Carlo simulations of a WLC in the absence of endpoint pinning or compressive forces. We initialize each chain as a rod of length *L* and generate trial configurations by

moving a randomly chosen monomer in a random direction sampled from a normal distribution with a mean zero and standard deviation 0.25a. The energy difference (ΔE) between the modified configuration and the previous configuration is calculated to check if the trial move is accepted or rejected. The configurations are accepted following the Metropolis criterion that says the probability of acceptance is directly proportional to the Boltzmann factor, $p_{\rm accept} = e^{-\beta \Delta E}$ with $\beta = 1/k_B T$. There are 10⁹ MC steps in between the initially grown chain and the final equilibrated chain configurations, which is the data used for plotting the end-to-end distance probabilities. A total of 1600 configurations are produced after equilibration.

To obtain the buckling statistics in the isometric ensemble, we pin the chain at the end-points in the x-direction so that the end-to-end distance is fixed (with $X_{ee} = xL$). For $X_{ee} \approx L$, the mean force applied to the filament is positive, stretching the filament in the x-direction. For sufficiently low X_{ee} , the mean force will become negative, and the chain will be compressed (and we expect the filament will buckle for some critical X_{ee}). We use the unpinned simulation method as described above to perform these simulations, modified to keep the end-to-end distance fixed by never selecting the endpoints as the monomers that are moved (\mathbf{r}_0 and \mathbf{r}_N are unchanged in all trial moves). We initialize the simulation with a rod of length $X_{ee} = 0.99L$ by compressing each bond vector's length by 1%. We equilibrated 5×10^4 configurations in two dimensions and \approx 8400 configurations in three dimensions by performing \approx 10⁹ MC steps per simulation. After equilibration, these configurations are compressed by 1% by reducing the length of each bond uniformly and equilibrating again. This procedure was followed reducing x by 0.01 at every iteration to x = 0.94 for two dimensions and x = 0.87for three dimensions.

III. RESULTS

A. The mean-field approach for wormlike chains

The MF method replaces rigid local constraints with averaged global constraints (as described in Sec. II A). A difficulty with the mean-field approach is determining the relationship between l_0 [the MF persistence length in Eq. (2)] and l_p [the true persistence length of the polymer in Eq. (1)]. With a priori knowledge of the exact mean squared curvature of the WLC, it is straightforward to use l_0 as an additional Lagrange multiplier,96 choosing the optimal value of l_0 by constraining $\left\langle \int_0^L ds \dot{\mathbf{u}}^2 \right\rangle_0$ to a known value. In this paper, we will generally not have this knowledge *a priori* and must find an approximate method for identifying a relationship between l₀ and l_p . In Ref. 100, the connection is made by recognizing that an unconstrained WLC has $\langle \mathbf{u}_0 \cdot \mathbf{u}_L \rangle_0 = e^{-3L/2l_0}$ in three dimensions, in comparison to the exact result $\langle \mathbf{u}_0 \cdot \mathbf{u}_L \rangle_{e,3} = e^{-L/l_p}$ (with $\langle \cdots \rangle_{e,3}$ the true statistical average in three dimensions). This suggests the replacement $l_0 = 3l_p/2$ in three dimensions. A similar calculation in two dimensions shows that $\langle \mathbf{u}_0 \cdot \mathbf{u}_L \rangle_0 = e^{-L/l_0}$ in comparison to the exact $(\mathbf{u}_0 \cdot \mathbf{u}_L)_{e,2} = e^{-L/2l_p}$, suggesting the substitution $l_0 = 2l_p$ in two dimensions. This substitution $l_0 = 3l_p/2$ in three dimensions has been used in multiple contexts; $^{93-95,100}$ we are not aware of this MF formalism utilized in two dimensions.

B. Distribution functions in two and three dimensions

An accurate derivation of the end-to-end distance distribution for a WLC using the MF theory has been previously accomplished in three dimensions. To our knowledge, an equivalent twodimensional distribution derived using this MF approach has not been reported in the literature, and we will compute it in this section. To determine the distribution function, we will find it convenient to define the Hamiltonian $H_1 = \frac{1}{2}l_1\int_0^L ds\dot{\mathbf{u}}^2 + \lambda\int_0^L ds\mathbf{u}^2 + \delta(\mathbf{u}_0^2 + \mathbf{u}_L^2),$ which is identical to the definition of H_0 in Eq. (2) but with a mean-field persistence length l_1 (with $l_1 \neq l_0$ in general). The distribution functions in two and three dimensions are determined by computing the constrained free energy $e^{-\mathcal{F}(\mathbf{R}_{ee})} = \int \mathcal{D}[\mathbf{u}(s)]$ $e^{-H_1 + \lambda L + 2\delta} \delta(\mathbf{R}_{ee} - \int_0^L ds \mathbf{u}(s)) = \left\langle e^{\lambda L + 2\delta} \delta(\mathbf{R}_{ee} - \int_0^L ds \mathbf{u}(s)) \right\rangle_1, \text{with } \langle \cdots \rangle_1$ being an average with respect to H_1 . The constraint of inextensibility is imposed on average by requiring $\partial \log[\mathcal{F}(\mathbf{R}_{ee})]/$ $\partial \lambda = \partial \log[\mathcal{F}(\mathbf{R}_{ee})]/\partial \delta = 0$. We can readily evaluate this via $e^{-\mathcal{F}(\mathbf{R}_{ee})} = e^{\lambda L + 2\delta} \int d^d \mathbf{q} e^{-i\mathbf{q}\cdot\mathbf{R}_{ee}} \left\langle \exp\left(i\mathbf{q}\cdot\int_0^L ds\mathbf{u}(s)\right)\right\rangle_1$. This calculation was performed in Ref. 100 in three dimensions and is straightforward in two dimensions by completing the square in the Hamiltonian, with $\lambda \int_0^L ds (\mathbf{u}^2 - i\mathbf{q} \cdot \mathbf{u}) = \mathbf{q}^2 L/2\lambda + \lambda \int_0^L ds \mathbf{v}^2$ for $\mathbf{v} = \mathbf{u} - i\mathbf{q}/2\lambda$. The path integrals can be evaluated using the propagator for the quantum harmonic oscillator in d-dimensions, with $Z(\mathbf{u}_0, \mathbf{u}_L; L) = (l_1 \Omega / 2\pi \sinh(\Omega L))^{d/2} \exp\left[-\frac{l_1 \Omega}{2} (\mathbf{u}_0^2 + \mathbf{u}_L^2) \coth(\Omega L)\right]$ $+ l_1 \Omega \mathbf{u}_0 \cdot \mathbf{u}_L \operatorname{csch}(\Omega L)$ and with $\Omega = \sqrt{2\lambda/l_1}$. The free-energy minimizing equations for δ and λ are unwieldy but are simplified considerably if we assume L is large and $\mathbf{R}_{ee}^2 = r^2 L^2$. Retaining terms of order L and replacing $\sinh(\Omega L) \approx \cosh(\Omega L) \approx e^{\Omega L}/2$ yields

$$\frac{2d}{2\delta + l_1\Omega} = 2, \qquad \Omega l_1(1 - r^2) = \frac{d}{2}, \tag{3}$$

in d=2 or 3 dimensions, with solutions $\Omega=d/2l_1(1-r^2)$ and $\delta=d(1-2r^2)/4(1-r^2)$. These values are substituted into the free energy $\mathcal{F}(r)=\frac{1}{d}\left(\frac{\pi^{1/2}l_1^2\Omega^{3/2}}{L^d}\right)^d\exp\left(-\frac{Ll_1\Omega^2}{2}(1-r^2)+\frac{dL\Omega}{2}+2\delta\right)$. We must normalize these distributions so that $L^d\int_0^1 d^d\mathbf{r} e^{-\mathcal{F}(\mathbf{r})}=1$

We must normalize these distributions so that $L^d \int_0^1 d^d \mathbf{r} e^{-\mathcal{F}(\mathbf{r})} = 1$. The integrals are straightforward to evaluate with the substitution $u = 1/(1-r^2)$, and $\mathbf{r} = \mathbf{R}_{ee}/L$ we find to leading order in L/l_p ,

$$P_{2d}(\mathbf{r}) = \frac{L^2 e^{L/2l_1}}{2\pi l_1 L(L+2l_1)} \frac{e^{-L/2l_1(1-|\mathbf{r}|^2)}}{(1-|\mathbf{r}|^2)^3},$$
 (4)

$$P_{3d}(\mathbf{r}) = \frac{3^6 L^{7/2} e^{9L/8l_1}}{2^{9/2} \pi^{3/2} (27L^2 + 72Ll_1 + 80l_1^2)} \frac{e^{9L/(8l_1(1-|\mathbf{r}|^2))}}{(1-|\mathbf{r}|^2)^{9/2}}.$$
 (5

Here, we neglect higher order contributions in L/l_1 , but we will find below that this leading order approximation is surprisingly accurate. Note that Eqs. (4) and (5) are vector distributions; when computing the distribution of the magnitude of the end-to-end distance, the volume elements $2\pi r$ or $4\pi r^2$ for two and three dimensions, respectively, should be included. Terms in the three-dimensional distribution differ from that in Ref. 100 because we have not replaced the mean-field persistence length l_1 in terms of the true persistence length l_p in Eq. (5) yet (discussed further below). The factor of δ plays a critical role in computing the distribution function by suppressing the excess fluctuations at the endpoints, as the end-to-end

distribution function would be $\propto (1 - |\mathbf{r}|^2)^{d/2}$ with $\delta = 0$ rather than $\propto (1 - |\mathbf{r}|^2)^{3d/2}$ we have found here.

C. The mean-field persistence length in two and three dimensions

As discussed in Sec. III A, the mean-field persistence length l₁ is not identical to the true persistence length of the chain, and without knowing an exact $\langle \int_0^L ds \hat{\mathbf{u}}^2 \rangle$, we cannot variationally determine l_1 explicitly. In Ref. 100, it is argued that we should expect $l_1 = l_0 = 3l_p/2$ for d = 3, based on the correlation function $\langle \mathbf{u}_0 \cdot \mathbf{u}_L \rangle_{d=3}$ = $e^{-3L/2l_0}$. End-to-end distributions for three-dimensional WLCs have been accurately recovered using Eq. (5) using this approximation. In two dimensions, a similar argument would suggest that l_1 should be replaced with $l_0 = 2l_p$ for d = 2. Surprisingly, we find a fairly poor agreement with the simulated end-to-end distance distribution functions of a two-dimensional WLC [the dashed lines in Figs. 1(a)-1(c)]: neither the mean nor the most probable end-to-end distances agree well with the simulated data with the substitution $l_1 = 2l_p$. The mean squared end-to-end distance is significantly underestimated in comparison to the simulations (see Table I). The most probable value r^{max} is also underestimated, and the probability of finding $r = r^{\text{max}}$ is also low compared to the simulations. This suggests that the distributions are not well predicted using the MF method with the substitution $l_1 = 2l_p$.

In order to improve the agreement, we instead choose l_1 such that $\langle \mathbf{r}^2 \rangle_{e,d} = \int d^d \mathbf{r} P(\mathbf{r})$, where $\langle \mathbf{r}^2 \rangle_{e,d}$ is the exact mean squared end-to-end distance for a WLC in d dimensions: $\langle \mathbf{R}^2_{ee} \rangle_{e,3} = 2Ll_p + 2l_p^2 (e^{-L/l_p} - 1)$ and $\langle \mathbf{R}^2_{ee} \rangle_{e,2} = 4Ll_p + 2l_p^2 (e^{-L/2l_p} - 1)$. These can be compared to the mean-squared end-to-end distances predicted by the MF theory in terms of l, with

$$\langle \mathbf{R}_{ee}^2 \rangle_{MF,2} = \int_0^1 dr \ 2\pi r^3 P_{2d}(r) = \frac{2L^2 l_1}{L + 2l_1},$$
 (6)

$$\langle \mathbf{R}_{ee}^2 \rangle_{MF,3} = \int_0^1 dr \ 4\pi r^4 P_{3d}(r) = \frac{4L^2 l_1 (9L + 20l_1)}{27L^2 + 72Ll_1 + 80l_1^2}.$$
 (7)

In two dimensions, equating the exact and MF predictions for the mean squared end-to-end distance yields

$$l_1 = l_p \frac{2\left(1 - 2\left(1 - e^{-L/2l_p}\right)\frac{l_p}{L}\right)}{1 - 4\frac{l_p}{l} + 8\left(1 - e^{-L/2l_p}\right)\frac{l_p^2}{l_p^2}}$$
 (2 dimensions). (8)

TABLE I. Comparison of the simulated and theoretical distributions using different values of I_1 : either $I_1 = 2I_p$ (equal to I_0 , predicted by the decay in the correlation function as described in Sec. III B) or defining I_1 using Eq. (8). We compute the ratio of the simulated vs MF mean squared end-to-end distances and the Kullback–Leibler divergence, D. Using Eq. (8) gives a much lower ratio of the simulated vs theoretical end-to-end distances and reduces D.

	$\langle R_{ee}^2 \rangle_{sim}/\langle R_{ee}^2 \rangle_{MF}$			K-L divergence D		
Quantity	$l_p = \frac{L}{2}$	$l_p = L$	$l_p = 2L$	$l_p = \frac{L}{2}$	$l_p = L$	$l_p = 2L$
Using $l_1 = 2l_p$ Using Eq. (8)	1.11 1.01	1.07 1.00	1.04 1.01	33.2 23.1	22.3 7.34	22.7 2.86

For flexible chains with $L\gg l_p$, we find that Eq. (8) reduces to $l_1\approx 2l_p$, recovering the substitution for the bending correlation functions to recover their unconstrained expected values. However, in the limit of $l_p\gg L$, Eq. (8) reduces to $l_1\approx 3l_p-L/8+O(l_p^{-1})$. This change in the coefficient (from 2 to 3) suggests that l_1/l_p may vary significantly with r for $l_p\gtrsim L$, and the substitution $l_1=2l_p$ would only be applicable in the limit of $l_p\to 0$. In Fig. 1(d), the solid line shows Eq. (8) as a function of l_p/L , and we see that significant deviations from $l_1/l_p=2$ occur even for moderate stiffnesses. Using l_1 as defined in Eq. (8), we find that the mean of the theoretical distribution matches the exact value of $\langle \mathbf{R}_{ee}^2 \rangle$, as given in Table I. We also compare the Kullback–Leibler (KL) divergence, $D=\sum_i P_{sim}(r_i)\log[P_{sim}(r_i)/P_{MF}(r_i)]$, between the simulated and theoretical distributions and find that D is significantly reduced when Eq. (8) is used to relate l_1 to l_p in Table I.

In three dimensions, solving for $\langle \mathbf{R}_{ee}^2 \rangle_{MF,3} = \langle \mathbf{R}_{ee}^2 \rangle_{e,3}$ leads to a more complicated expression for the relationship between l_1 and l_p , which is easily evaluated numerically. We find $1.35 \le l_1/l_p \le 1.5$ in three dimensions, as shown in Fig. 1(d). The numerical differences for stiff and flexible chains are much smaller in three dimensions than in two dimensions and suggest that using $l_1 \approx 3l_p/2$ for the MF persistence length may be approximately valid even for stiff chains (consistent with Ref. 100). The agreement in three dimensions is shown in Fig. 1(e) for $l_p/L = 1$ and agrees well.

D. Buckling of a compressed filament

To estimate the end-to-end distance at which the chain will buckle, we determine the distribution function for the transverse position of a filament pinned at both endpoints, with the expectation that the emergence of a bimodal distribution indicates a buckling transition [sketched in Fig. 2(c)]. In two and three dimensions, we assume the end-to-end distance to be in the x-direction with magnitude X_{ee} and wish to compute the y-position along the backbone at s (Y_s). In two dimensions, this distribution can be determined by computing

$$P(Y_s; X_{ee}) = \left(\delta \left(X_{ee} - \int_0^L ds u_x\right) \delta \left(\int_0^L ds u_y\right) \times \delta \left(Y_s - \int_0^s ds' u_y(s')\right)\right), \tag{9}$$

where $\mathbf{u} = \dot{\mathbf{r}} = (u_x, u_y)$ is the tangent vector. In three dimensions, a similar expression can be developed including an additional term $\delta(\int_0^L ds u_z(s))$ in the average. Note that in two and three dimensions, we do not impose a constraint on the direction of the pinned bonds [that is, $\mathbf{u}(0)$ and $\mathbf{u}(L)$ are not constrained to be aligned with the x axis]. This assumption is discussed in more detail in the conclusions. This average is readily evaluated using the Fourier transform,

$$P(Y_s; X_{ee}) = \int \frac{d^d \mathbf{k} dq}{(2\pi)^{d+1}} e^{-i\mathbf{k}\cdot\mathbf{R}_{ee}-iqY_s} \exp \times \left(i\mathbf{k}\cdot\int_0^L ds'\mathbf{u}(s') + iq\int_0^s ds'u_y(s')\right) e^{-\beta H_1}, \quad (10)$$

with $\mathbf{R}_{ee} = (X_{ee}, 0)$ in two dimensions and $(X_{ee}, 0, 0)$ in three dimensions. Because the MF Hamiltonian is quadratic, the integral can be evaluated in a straightforward fashion. As was the case for the

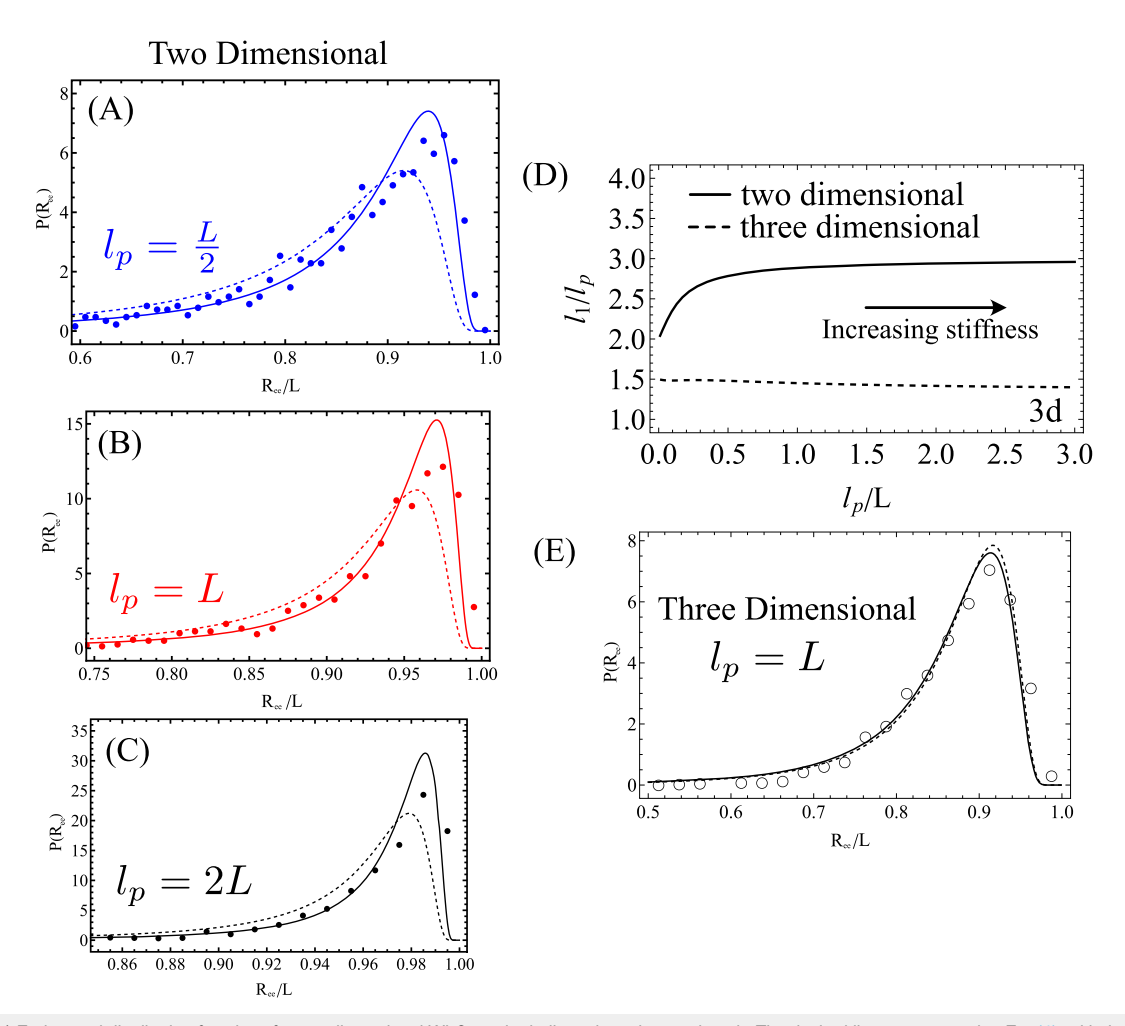


FIG. 2. (a)–(c) End-to-end distribution functions for two-dimensional WLCs at the indicated persistence length. The dashed lines correspond to Eq. (4), with the substitution $I_1 = 2I_p$, while the solid lines correspond to the substitution in Eq. (8) $[(a)-(c) I_1 \approx 2.78I_p, I_1 \approx 2.92I_p, and I_1 \approx 2.96I_p]$. A significant improvement in the agreement is observed using Eq. (8), consistent with Table I. The filled points in plots (a)–(c) represent simulation data for the end-to-end distances for different stiffness parameters in two dimensions. Note the change in the x axes in (a)-(c), which gives rise to greater noise in (a) than in (c). (d) The ratio I₁/I_p in two (black solid line) and three (black dashed line) dimensions. In three dimensions, I_1/I_p is weakly varying between 1.35 and 1.50. In two dimensions, the change is more significant (varying between 2 and 3), leading to the differences seen in the dashed lines in (a)–(c). (e) End-to-end distribution functions for $I_p = L$ in three dimensions. The dashed lines correspond to Eq. (5) with the substitution $I_1 = \frac{3}{2}I_p$, while the solid lines correspond to the choice of I_1 such that $\langle \mathbf{R}_{ee}^2 \rangle_{MF,3} = \langle \mathbf{R}_{ee}^2 \rangle_{e,3}$. In three dimensions, the distributions are nearly identical using either definition for \tilde{l}_1 , suggesting that the MF theory does not depend sensitively on the method by which l_1 is chosen in three dimensions, consistent with (d). The open points in the plot represent simulation data for the end-to-end distance in three dimensions.

end-to-end distribution function, it is extremely useful to take the limit of $L \gg 0$ so that the hyperbolic trigonometric functions can be replaced with exponentials. We further assume that $e^{s\Omega/2} \gg e^{-s\Omega/2}$, meaning the point s is far from the endpoints. In this limit, we find after some algebra that, in d = 2 or 3 dimensions, the distribution function is

$$\begin{split} P(Y_s; X_{ee}) & \propto \frac{\Omega^{3d/2} e^{2\delta - dL\Omega/2 + l_1 L\Omega^2/2}}{(2\delta + l_1\Omega)^d g^{1/2}(\Omega)} \\ & \times \exp\left(-\frac{l_1 X_{ee}^2 \Omega^2}{2L} + \frac{L l_1 Y_s^2 \Omega^2}{g(\Omega)}\right), \end{split} \tag{11}$$

with $g(\Omega) = 1 - 2s(1 - \frac{s}{L})\Omega$. It is convenient to write $X_{ee} = xL$, $Y_s = yL$, and $s = \sigma L$. Taking the limit of $L \to \infty$ imposing the inextensibility constraints on average using $\partial \log(P)/\partial \delta = \partial \log(P)/\partial \delta$ $\partial \lambda = 0$ gives the mean-field solutions,

$$\delta = \frac{d}{2} - \frac{l_1 \Omega}{2}, \quad \Omega = \frac{d}{2l_1} \left(1 - x^2 - \frac{y^2}{\sigma(1 - \sigma)} \right)^{-1}.$$
 (12)

The substitution of Eq. (12) into Eq. (11) gives the distributions to the leading order in L,

$$P(y;x) \propto \left(1 - x^2 - \frac{y^2}{\sigma(1 - \sigma)}\right)^{-3d/2 - 1} \times \exp\left[\frac{(2d - 3)L}{2l_1} \left(1 - x^2 - \frac{y^2}{\sigma(1 - \sigma)}\right)^{-1}\right].$$
(13)

These distributions cannot be integrated analytically in terms of elementary functions [unlike the case of the end-to-end distribution function in Eq. (4) or (5)], and we will numerically evaluate the normalization factor.

The length of the chain fluctuates in the simulations with the length of the *k*th simulated filament defined as $L_k = \sum_i |\mathbf{r}_i^{(k)} - \mathbf{r}_{i-1}^{(k)}|$, while Eq. (13) assumes that the filament has a fixed length L. In order to compare the theory directly to simulations, in Fig. 3, we show the distribution of $y = Y_{L/2}/L$ for only data with 0.999 < L_k/L < 1.001 (selecting only ≈10% of our simulated configurations with an approximately fixed length; length fluctuations will be accounted for in Sec. III E). We plot the distribution in Eq. (13) with l_1 defined in Eq. (8) and see that the distribution is well predicted by the theory for (almost) constant L. When $x = X_{ee}/L \approx 1$, the distributions are unimodal and peak around y = 0, while bimodal distributions are observed when x is sufficiently small. These bimodal distributions indicate that the filament has buckled: the most probable location is not centered at $Y_{L/2} = 0$ but instead at a finite value. The distribution functions have critical points as a function of y at $y_* = 0$ or $y_* = \pm \left(\frac{1-x^2}{4} - \frac{c_d L}{4l_1}\right)^{1/2}$ with $c_d = 1/8$ in two dimensions and $c_d = 3/11$ in three dimensions. The nonzero peaks become real when $x < x_* = \left(1 - \frac{c_d L}{l_1}\right)^{1/2}$ with x_* being the critical compressed distance at which buckling occurs. Buckling is a continuous phase transition as shown in Fig. 4(a), with $y_* = 0$ when $x \ge x_*$, consistent with the observations in Ref. 73. The phase diagram of the buckling is shown in Fig. 4(b) for both two and three dimensions. The onset of buckling occurs for larger x_* in two dimensions than in three dimensions; for our parameters of $l_p \approx L$, the buckling occurs at $x_* \approx 0.978$ in two dimensions and $x_* = \frac{3}{\sqrt{11}} \approx 0.905$ in three dimensions. Note that we also predict that the buckling will not occur for sufficiently flexible

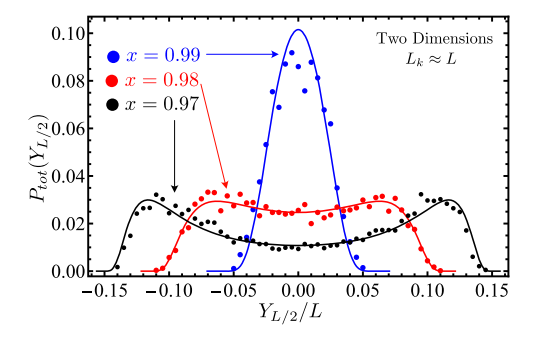


FIG. 3. Transverse position distribution of the midpoint of a two-dimensional filament with $I_p = L$. Points represent the y component of the midpoint of the simulated data for which the length of the kth simulated chain is $L_k \approx (N-1)a$ (permitting variations of around 0.1%), and lines correspond to the predictions of Eq. (13), replacing I_1 with Eq. (8). Note that there are no free parameters in the fitting. Blue refers to $X_{ee}/L = 0.99$, red 0.97, and black 0.95.

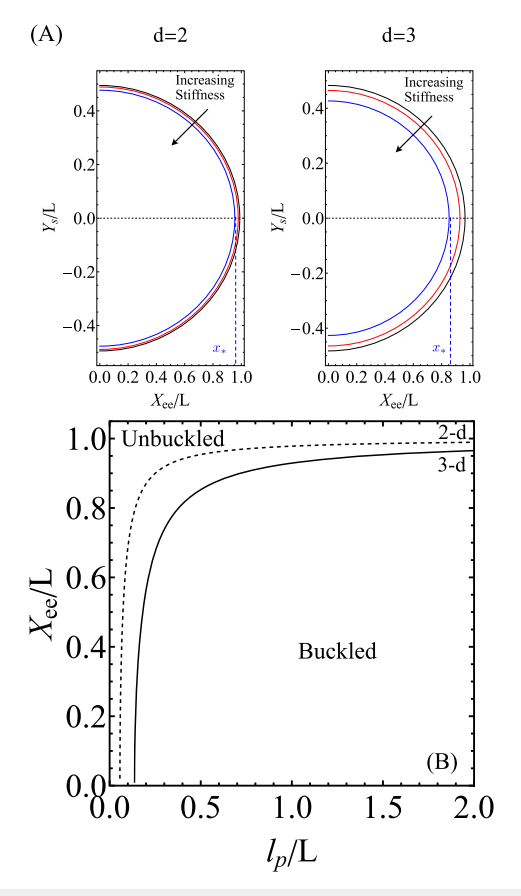


FIG. 4. (a) The most probable value of the transverse position of the midpoint of the polymer in two and three dimensions, with $I_p = L/2$ (blue), L (red), and 2L (black). Buckling occurs when the most probable value of the transverse position is non-zero (when $x = x_* = \sqrt{1 - c_d L/I_1}$). (b) Phase diagram of the transition between unbuckled and buckled filaments. The transition occurs at an earlier compression value (X_{ee}/L) for more flexible chains in two dimensions than in three dimensions, and in either dimensionality, there is a minimum persistence length required for buckling to occur. In two and three dimensions, stiff chains will buckle at a critical compression and the value occurs earlier for two dimensions than for three dimensions.

chains (when $l_1/L \le c_d$) since x_* is imaginary for low l_1 . In terms of the true persistence length, this corresponds to $\frac{l_p}{L} \approx 0.056 = \alpha_2$ in two dimensions and $\frac{l_p}{L} = \frac{2}{11} \approx 0.182 = \alpha_3$ in three dimensions. Pinning the endpoints of a wormlike chain fixes the end-to-end

Pinning the endpoints of a wormlike chain fixes the end-to-end distance, and thus, the compressive force fluctuates. This is distinct from the problem of Euler buckling, which predicts a first-order phase transition in the $T \to 0$ limit. We can readily compute the mean compressive force via $L\beta\langle f \rangle = -\partial \log[P(r)]/\partial r$ and find

$$L\beta(f(x)) = -\frac{8x}{(1-x^2)} + \frac{Lx}{l_1(1-x^2)^2} + \frac{1}{x}$$
 2 dimensions (14)

$$= -\frac{(1-9x^2)}{x(1-x^2)} + \frac{Lx}{l_1(1-x^2)^2} + \frac{2}{x} \quad \text{3 dimensions.} \quad (15)$$

These forces are shown in Fig. 5 with the substitution of Eq. (8) for l_1 in two dimensions [Fig. 5(a)] and $l_1 = 3l_p/2$ in three dimensions [Fig. 5(b)]. As expected, for $x \approx 1$, the mean forces are positive and elongate the chain. The onset of the compressive forces is earlier in two dimensions than in three, at a higher compression ratio x [as in Fig. 4(b)]. The substitution of $x = x_*$ into Eqs. (14) and (15) give a mean compressive force $\langle f(x_*) \rangle = -\frac{33k_BTl_p}{8L^2} \sqrt{1 - \frac{2L}{11l_p}}$ in three dimensions. The standard Euler buckling result at T = 0predicts a critical force at^{73,99} $f_E = -\pi^2 \frac{k_B T l_p}{L^2}$. Our theoretical prediction, thus, gives the same scaling of the mean compressive force with l_p and L as has been used previously. The scaling coefficient, $\langle f(x_*) \rangle \approx -\frac{33}{8} \frac{k_B T l_p}{L^2}$, is about 60% lower than the standard Euler buckling coefficient in the limit of $l_p \to \infty$. Reference 73 finds that the critical buckling force on a wormlike chain falls somewhere between $0.67 f_E$ and $1.33 f_E$ in the presence of thermal fluctuations and a constant compressive force. This apparent inconsistency is due to the fact that we use a fixed end-to-end distance (Helmholtz) ensemble rather than a fixed force (Gibbs) ensemble. It is also worth noting that the scaling coefficients in the mean-field approach are expected to be correct within an order of magnitude. A surprising result in two dimensions is that we find $f(x_*) = k_B T / L \sqrt{1 - c_d L / l_1}$,

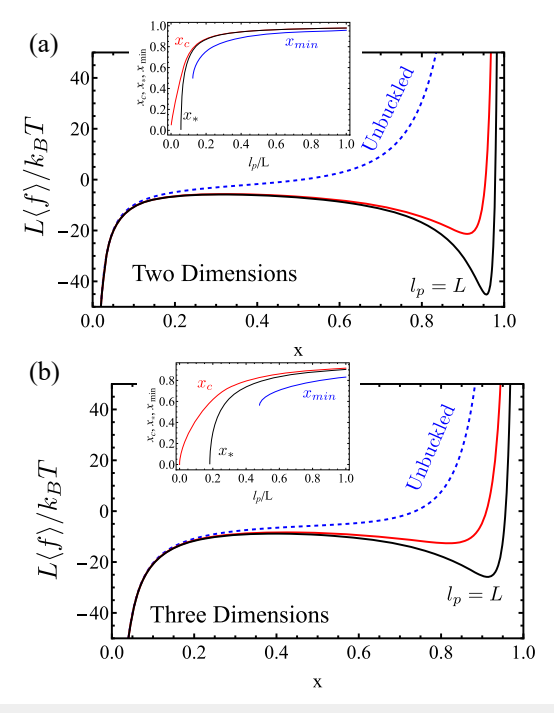


FIG. 5. Mean force on the filaments in two (a) and three (b) dimensions as a function of the fixed extension $x = X_{ee}/L$. Shown are $I_p/L = 1$ (black) and 1/2 (red), as well as the stiffnesses α_d at which the buckling does not occur (blue dashed line). The insets for each show the extension at which the force becomes compressive (x_c) , the extension at which the phase transition occurs (x^*) , and the location of the local minimum of the force (x_{\min}) as a function of stiffness. Buckling does not coincide with the minimum in the compressive forces, and in two dimensions, the onset of buckling is very close to the onset of compression even for fairly flexible chains.

with the scaling coefficient of the l_p/L^2 term vanishing. We, thus, do not recover the scaling for the Euler buckling in two dimensions but rather find that the onset of the buckling transition occurs when the mean compressive force is $\approx -k_BT/L$ for stiff chains (discussed below). This again may be due to inaccuracies in the scaling coefficient; if $c_2 \neq 1/8$, the usual Euler buckling scaling re-emerges with a different scaling coefficient.

In the insets in Fig. 5, we show the extension at which the forces become compressive (x_c , the compression at which 14 or 15 become negative), the onset of buckling at x_* , and the location of the local minimum of the force (x_{\min}) . We see the buckling transition occurs between the onset of compression and the local minimum, but for stiff chains $x_* \approx x_c$, this means that the chains of even moderate stiffness buckle almost immediately in two dimensions when a mean compressive force is applied. In three dimensions, the buckling transition is between the onset of compression and the local minimum, but $x_* \not\approx x_c$ unless the chains are very stiff. In both two and three dimensions, the local minima in the compressive forces do not coincide with the onset of the buckling transition. Much like the absence of the buckling for sufficiently flexible chains, we see these local minima in the compressive forces cease to exist for sufficiently low l_p/L . It is interesting to note that the scaling coefficient of the Euler buckling solution is independent of the dimensionality⁷³ $(f_E = -\pi^2 k_B T l_p/L^2)$ in two and three dimensions) since the actionminimizing $\vec{T} = 0$ solution has a constant azimuthal angle. Here, we see that the dimensionality does affect the scaling coefficient of the compressive force at finite T with fixed endpoints (rather than constant force).

E. Accounting for fluctuations in length

The distribution in Eq. (13) assumes a fixed L, but all biomolecules have a finite stretch modulus, and many computational models (including our MC algorithm) permit length fluctuations. For example, F-actin has a stretch modulus 107 of $\approx 1.8 \times 10^9$ N/m², which allows for around 1%-5% length fluctuations. In Fig. 6, we show that the theoretical prediction in Eq. (13) (dashed lines) in two and three dimensions fails to capture the simulated distribution $P(Y_{L/2})$ for large x (stretching) but appears to perform well for small x (compression). The two-dimensional simulation includes 50 000 simulated configurations for each distribution, and for three dimensions, there are ~8400 simulated configurations for each distribution. For both compression and stretching, we see that the simulated length of the chain for the kth simulation, $L_k = \sum_{i=1}^{N-1} |\mathbf{r}_{i+1}^k - \mathbf{r}_i^k|$, varies by $\approx 2\%$ (insets in Fig. 6) and the average length is increased when stretched (because the locations of the peaks of the length distributions increase with x) but not when compressed. The length distributions are all well-fit by a normal distribution, $p(L_{sim}) = \exp[(L_{sim} - \bar{L})^2/2\sigma_L^2]/\sqrt{2\pi\sigma_L^2}$ (the solid curves in the inset) with \bar{L} and σ_L^2 being the mean and variance of the simulated length, respectively. An exact calculation of \bar{L} and σ_L is difficult analytically due to the constraint of fixed distance in the x-direction, and we simply calculate them from the data directly. In computing \bar{L} and σ_L , we exclude extensions that occur less than 0.1% of the data due to rare events of high compression of the bonds when x is small.

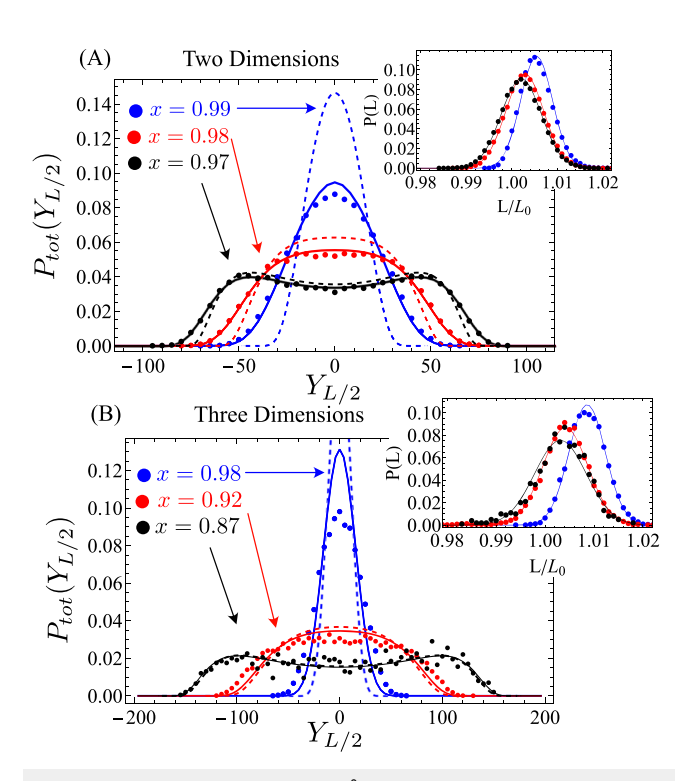


FIG. 6. Simulated distributions with $\kappa_s/a^2=10k_BT$ (points) in comparison to the fixed length distributions in Eq. (13) (dashed lines) and Eq. (16) (solid lines) in two (a) and three (b) dimensions. Points represent the transverse component of the midpoint of the simulated data (y axis in two dimensions and y and z axes in three dimensions). The insets show the distributions of the simulated lengths, which are well fit by a Gaussian. $L_0=(N-1)a$ is the length of the chain and $L=L^k$ is the length of the chain for the kth simulation. The transition between the buckled and unbuckled states differs in two and three dimensions, and different values of compression are shown: (a) x=0.99 (blue), 0.98 (red), and 0.97 (black), and (b) x=0.98 (blue), 0.92 (red), and 0.86 (black). Note that, in (b), the peak of the blue dashed line is cut off to improve visualization.

Initially, we tested to see if we could fit the simulated distributions using Eq. (13) with L and l_p as fitting parameters but found that the fitted distributions still did not agree well (data not shown). To better match the simulations, we compute the total distribution accounting for length fluctuations,

$$P_{tot}(y;x) = \int_{L_{min}}^{L_{max}} dL_{sim} \ p(L_{sim}) \ \frac{P(yL_{sim};xL_0)}{\mathcal{N}(L_{sim},L_0)}, \tag{16}$$

with the Gaussian prior P(L) in the insets in Fig. 6, $L_0 = (N-1)a$ being the length of the chain for $\kappa_s \to \infty$, and the normalization $\mathcal{N}(L_{sim}, L_0) = \int_{Y_{\min}}^{Y_{\max}} dY P(y L_{sim}, x L_0)$. This integral must be evaluated numerically. The bound values of L, L_{\min} and L_{\max} , are chosen such that $\int_{-\infty}^{L_{\min}} dL p(L) = \int_{L_{\max}}^{\infty} dL p(L) = 10^{-5}$ (ignoring low-probability lengths) and $Y_{\max} = -Y_{\min} = (L_{sim}/2)\sqrt{1-x^2}$. The numerical integration uses a 25-point Gaussian quadrature, and the resulting distributions are shown as the solid lines in Fig. 6. The fixed length distribution functions in Fig. 6 badly fail to capture the

simulated distributions for x = 0.99 [two dimensions, blue dashed lines in Fig. 6(a)] or 0.98 [three dimensions, blue dashed lines in Fig. 6(b)], while the convolved distributions P_{tot} show improved agreement. There is still some difference between the theory and simulations for large x, which may be due to the failure of a Gaussian theory to accurately describe a strongly stretched inextensible chain.¹⁰⁸ In two dimensions, the convolved distribution in Eq. (16) agrees almost perfectly with the simulations while the fixed length theory fails to capture the tails well. In three dimensions, the agreement for the fixed length theory is nearly quantitative below the buckling transition, suggesting that the theory can be reliably used for high compression in three dimensions. The agreement between the fixed-length theory in Eq. (13) and the convolved distribution in Eq. (16) suggests that our predictions of the location of the buckling transition will be accurate even for systems with finite stretching modulus.

IV. DISCUSSION AND CONCLUSIONS

In this paper, we have studied the statistics of semiflexible filaments compressed due to pinning at the endpoints (in the Helmholtz ensemble) to better understand the buckling of stiff polymers when compressed. We find that there is a continuous phase transition for a pinned polymer in both two and three dimensions, transitioning from configurations that thermally fluctuate around the compression axis for high extensions $(x = X_{ee}/L \gtrsim x_*)$ to thermal fluctuations about bent configurations for strong compression $(x < x_*)$. This transition does not precisely coincide with the change in the sign of the mean force (although is very close in two dimensions) nor does it coincide with the point at which the compressive force experiences a local minimum. For rigid chains, all three of these points nearly coincide, consistent with the observations in Ref. 48 (with $L/l_p \approx 117$). We predict that even fairly flexible chains may also buckle (with L/l_p as low as 0.1 or 0.2 in two or three dimensions, respectively), but the buckling transition will occur only for $X_{ee} \approx 0$ for such a low l_p .

We have shown that the buckling transition at a finite temperature is a continuous transition in the isometric ensemble. However, first-order transitions are directly related to energy dissipation and the phenomenon of hysteresis that has been observed in the buckling of biopolymers. 15,16,109 To better understand the predictions of our model, we can draw an analogy between our system and the Ising model. At a zero applied external field and below the critical temperature, the spins in a ferromagnetic material align and show spontaneous magnetization to a positive or a negative value. Above the critical temperature, thermal fluctuations are sufficiently high to prevent global alignment in two and three dimensions. In our system of a buckled semiflexible polymer under compression, the analogous order parameter to temperature in an Ising model is the level of compression, $x = X_{ee}/L$, with the transverse position Y_s playing an analogous role to the magnetization. In Fig. 4(a), the most probable value of the transverse position of the midpoint of the polymer, Y_s , is plotted with the order parameter, x. This figure indicates that, above the critical compression, there is no buckling and the chain fluctuates around a flat chain configuration but buckling sets in below the critical compression and the chain fluctuates around a laterally curved configuration, either in the positive or

negative transverse direction. The distribution functions indicate a continuous phase transition in Fig. 6, which transitions from unimodal to bimodal, and in Fig. 5 where the mean compressive force is non-monotonic.

In addition to the spontaneous magnetization below the critical temperature, an applied field can provide a preferred direction for the spins to point in the Ising model. If the external field changes its direction abruptly, the sign of the magnetization in the spins may also change abruptly. The discontinuous jump in the magnetization is a sign of a first-order transition. Energy dissipation and the phenomenon of hysteresis 17,110-112 in first-order transitions are associated with the existence of meta-stable states 113,114 resulting from the past direction of the external field. Analogously, for the case of buckling in semiflexible polymers and for a compression level, $x < x_*$, the polymer is already in a buckled state either in the positive or the negative transverse direction. Introducing an external field or deformation forces like shear, 55,111,112,115 in the transverse direction (y direction for two dimensions and y and z directions for three dimensions) can lead to an abrupt jump and change the direction of the most probable value of the transverse position of the midpoint of the polymer. Thus, to observe a discontinuous transition in our model for buckling, it is necessary to introduce a transverse external field that may include hydrodynamic interactions or cross-links between filaments in a network. 15,16

Hysteresis plays a pivotal role in mechanical buckling in biological systems, ^{17,109,112} and a time-varying transverse external field in our model will result in meta-stable states where the polymer retains the memory of its initial condition (buckling in the transverse direction to the compression axis). Recent work¹⁰⁹ has also shown that cross-linked actin networks found in the cytoskeleton can exhibit mechanical hysteresis due to direction-dependent response to shear. The degree of hysteresis in these semiflexible polymer networks can exhibit adaptive behavior in the cytoskeleton. It was found that the adaptivity of these networks can be tuned through the cross-linker concentration and type. It will be interesting to explore the same behavior for a simple model of cross-linked actin filaments under compression, a planned avenue for future work.

The stiffness of many biopolymers plays an essential role in the structure and dynamics of compressed filamentous networks and bundles, as demonstrated both theoretically 17 and experimentally. 3,15,16,53,75,80,116 The persistence length of these molecules is central to characterizing their behavior when compressed. In this work, we have derived a relation between the mean-field persistence length obtained from our theory, and while we found that, in three dimensions, the very simple relation $l_1 = 3l_p/2$ agrees well with simulated data, modeling a two-dimensional buckled filament requires a nonlinear relationship between l_1 and l_p . The novel two-dimensional end-to-end distribution function predicted here may be relevant to studying the statistics of surface-bound filaments or networks. We also found that the distributions are quite sensitive to variations in length for stretched filaments, and the theory does a relatively poor job of capturing the distributions for the normalized extension $X_{ee} \approx (N-1)a$. In three dimensions, we find that the theory and simulations agree well for smaller x (closer to the buckling transition), and the inextensible theory is likely sufficient for understanding the statistics of filaments with finite stretching

moduli, such as F-actin. In two dimensions, we found that the inextensible theory only qualitatively captures the simulated distributions and one must account for length fluctuations explicitly to quantitatively describe the distributions. Despite this sensitivity in the distributions, the compression at which buckling occurs predicted by the inextensible theory $(x_* = \sqrt{1 - c_d L/l_1})$ is expected to be accurate in both two and three dimensions.

In this paper, we have pinned the endpoints of the filament in one dimension and induced buckling by decreasing the end-toend distance along that axis. This imposes no constraint on the direction of the bonds at the endpoints, but in many biologically or experimentally relevant conditions, one might expect constraints on the statistics of the endpoints. 20-22,80 These may include rigid constraints of clamped (both endpoints normal to a surface) or cantilevered (one end normal to a surface and the other free) ensembles, but other softer constraints might be appropriate depending on the system. In this paper, we also showed that our finite-size isometric system does not precisely coincide with the isotensional system. With $f_c \approx \pi^2 k_B T l_p / \hat{L}^2$ being the critical force for buckling of a stiff chain,⁸¹ we found that the mean buckling force $\langle f \rangle \neq f_c$ at the critical compression x_* in three dimensions. While we did find that $\langle f \rangle_{MF,3}$ has the same scaling of $f_c \propto l_p/L^2$ in three dimensions, we surprisingly found, in two dimensions, that at the critical compression x_* , the scaling of $\langle f \rangle_{MF,2} \propto / l_p/L^2$. We are not aware of an explicit calculation of the buckling statistics of a wormlike filament in two dimensions with a constant compression force, so it is not clear whether the scaling of our isometric result is consistent with the isotensional ensemble. More work is needed to fully understand the equivalence of these two ensembles in the thermodynamic limit. It is certainly possible to include rigid constraints at the endpoints by computing averages as $\langle \cdots \rangle_{clamped} = \langle (\cdots) \delta(\mathbf{u}_0 - \hat{x}) \delta(\mathbf{u}_L - \hat{x}) \rangle_1$, and we readily find that $\Omega_{clamped} = d/2l_p(1-x^2-y^2/\sigma(1-\sigma))$ to leading order in L, identical to the value of Ω found for free ends. Unsurprisingly, the mean-field solution for the extensive contribution to the free energy is independent of the endpoint constraints in the limit as $L \to \infty$ and suggests the buckling transition will occur at the same value of *x* regardless of the endpoint conditions. However, a weakness in the mean-field approach when studying such endpoint constraints is how to handle terms in the free energy involving δ , which suppresses endpoint fluctuations. In the absence of fluctuations at the endpoints, we expect $\delta \to \infty$. Rigidly constraining the endpoints and minimizing the resulting free energy yield an expression for δ that is an unwieldy function of x and y. We find that $\delta \propto L$ under clamped conditions (consistent with the expectation of $\delta \to \infty$ since *L* is assumed large) and also find that δ diverges when Ω diverges [when $y = \sqrt{(1-x^2)/\sigma(1-\sigma)}$]. The extensive scaling of δ significantly complicates the analysis on the mean-field level. While an interesting direction for future work would compare the meanfield predictions in the clamped case to simulations and develop an analytically tractable functional form, significant numerical work and simulations are required to better understand the effect of rigid bond boundary constraints.

ACKNOWLEDGMENTS

We are grateful to the members of the active-cytoskeleton focus group at the Center for Theoretical Biological Physics (CTBP) for stimulating discussions on a broad range of topics involving the modeling of F-actin. A.M. also benefited greatly from feedback from her doctoral committee members for this project. This work was completed in part with resources provided by the Research Computing Data Core at the University of Houston. We acknowledge funding from the National Science Foundation (Grant No. NSF-PHYS-2019745) supporting this work as well as computational resources through Grant No. NSF-CNS-1338099.

AUTHOR DECLARATIONS

Conflict of Interest

The authors have no conflicts to disclose.

Author Contributions

Ananya Mondal: Conceptualization (supporting); Formal analysis (equal); Investigation (equal); Methodology (supporting); Software (lead); Validation (equal); Visualization (supporting); Writing – original draft (equal); Writing – review & editing (supporting). Greg Morrison: Conceptualization (lead); Formal analysis (equal); Funding acquisition (lead); Investigation (equal); Methodology (lead); Project administration (lead); Resources (lead); Software (supporting); Supervision (lead); Validation (equal); Visualization (lead); Writing – original draft (equal); Writing – review & editing (lead).

DATA AVAILABILITY

The data that support the findings of this study are available from the corresponding author upon reasonable request.

REFERENCES

- ¹M. Murrell, P. W. Oakes, M. Lenz, and M. L. Gardel, "Forcing cells into shape: The mechanics of actomyosin contractility," Nat. Rev. Mol. Cell Biol. **16**, 486–498 (2015)
- ²K. D. Costa, W. J. Hucker, and F. C.-P. Yin, "Buckling of actin stress fibers: A new wrinkle in the cytoskeletal tapestry," Cell Motil. **52**, 266–274 (2002).
- ³M. Bathe, C. Heussinger, M. M. A. E. Claessens, A. R. Bausch, and E. Frey, "Cytoskeletal bundle mechanics," Biophys. J. **94**, 2955–2964 (2008).
- ⁴E. M. De La Cruz and M. L. Gardel, "Actin mechanics and fragmentation," J. Biol. Chem. **290**, 17137–17144 (2015).
- ⁵Y. Bashirzadeh, N. H. Wubshet, and A. P. Liu, "Confinement geometry tunes fascin-actin bundle structures and consequently the shape of a lipid bilayer vesicle," Front. Mol. Biosci. 7, 610277 (2020).
- ⁶Y. Bashirzadeh, S. A. Redford, C. Lorpaiboon, A. Groaz, H. Moghimianavval, T. Litschel, P. Schwille, G. M. Hocky, A. R. Dinner, and A. P. Liu, "Actin crosslinker competition and sorting drive emergent GUV size-dependent actin network architecture," Commun. Biol. 4, 1136 (2021).
- ⁷J. Borovac, M. Bosch, and K. Okamoto, "Regulation of actin dynamics during structural plasticity of dendritic spines: Signaling messengers and actin-binding proteins," Mol. Cell. Neurosci. **91**, 122–130 (2018).
- ⁸K. Runge, C. Cardoso, and A. de Chevigny, "Dendritic spine plasticity: Function and mechanisms," Front. Synaptic Neurosci. **12**, 36 (2020).
- ⁹G. Jacquemet, H. Hamidi, and J. Ivaska, "Filopodia in cell adhesion, 3D migration and cancer cell invasion," Curr. Opin. Cell Biol. **36**, 23–31 (2015).

- ¹⁰ A. Calzado-Martín, M. Encinar, J. Tamayo, M. Calleja, and A. San Paulo, "Effect of actin organization on the stiffness of living breast cancer cells revealed by peak-force modulation atomic force microscopy," ACS Nano 10, 3365–3374 (2016).
- ¹¹ A. Mogilner and B. Rubinstein, "The physics of filopodial protrusion," Biophys. J. 89, 782–795 (2005).
- ¹² H. Mellor, "The role of formins in filopodia formation," Biochim. Biophys. Acta, Mol. Cell Res. **1803**, 191–200 (2010).
- ¹³T. Bornschlögl, "How filopodia pull: What we know about the mechanics and dynamics of filopodia," Cytoskeleton **70**, 590–603 (2013).
- ¹⁴ K. Katoh, K. Hammar, P. J. S. Smith, and R. Oldenbourg, "Arrangement of radial actin bundles in the growth cone of *Aplysia* bag cell neurons shows the immediate past history of filopodial behavior," Proc. Natl. Acad. Sci. U. S. A. **96**, 7928–7931 (1999).
- ¹⁵O. Lieleg, M. M. A. E. Claessens, Y. Luan, and A. R. Bausch, "Transient binding and dissipation in cross-linked actin networks," Phys. Rev. Lett. **101**, 108101 (2008).
- ¹⁶O. Lieleg, M. M. A. E. Claessens, and A. R. Bausch, "Structure and dynamics of cross-linked actin networks," Soft Matter 6, 218–225 (2010).
- ¹⁷C. P. Broedersz and F. C. MacKintosh, "Modeling semiflexible polymer networks," Rev. Mod. Phys. 86, 995 (2014).
- ¹⁸Y. Mulla, F. C. MacKintosh, and G. H. Koenderink, "Origin of slow stress relaxation in the cytoskeleton," Phys. Rev. Lett. 122, 218102 (2019).
- ¹⁹D. Strehle, J. Schnauß, C. Heussinger, J. Alvarado, M. Bathe, J. Käs, and B. Gentry, "Transiently crosslinked F-actin bundles," Eur. Biophys. J. 40, 93–101 (2011).
- ²⁰C. P. Brangwynne, F. C. MacKintosh, S. Kumar, N. A. Geisse, J. Talbot, L. Mahadevan, K. K. Parker, D. E. Ingber, and D. A. Weitz, "Microtubules can bear enhanced compressive loads in living cells because of lateral reinforcement," J. Cell Biol. 173, 733–741 (2006).
- ²¹O. Chaudhuri, S. H. Parekh, and D. A. Fletcher, "Reversible stress softening of actin networks," Nature 445, 295–298 (2007).
- ²²S. L. Freedman, S. Banerjee, G. M. Hocky, and A. R. Dinner, "A versatile framework for simulating the dynamic mechanical structure of cytoskeletal networks," Biophys. J. 113, 448–460 (2017).
- ²³ J. Berro, A. Michelot, L. Blanchoin, D. R. Kovar, and J.-L. Martiel, "Attachment conditions control actin filament buckling and the production of forces," Biophys. J. **92**, 2546–2558 (2007).
- ²⁴ J.-L. Martiel, A. Michelot, R. Boujemaa-Paterski, L. Blanchoin, and J. Berro, "Force production by a bundle of growing actin filaments is limited by its mechanical properties," Biophys. J. 118, 182–192 (2020).
- 25 N. Khanduja and J. R. Kuhn, "Processive acceleration of actin barbed-end assembly by N-WASP," Mol. Biol. Cell 25, 55–65 (2014).
- ²⁶W. Xu, X. Liu, and X. Liu, "Modeling the dynamic growth and branching of actin filaments," Soft Matter 18, 3649 (2022).
- ²⁷ M. Lenz, T. Thoresen, M. L. Gardel, and A. R. Dinner, "Contractile units in disordered actomyosin bundles arise from F-actin buckling," Phys. Rev. Lett. 108, 238107 (2012).
- ²⁸P. Ronceray, C. P. Broedersz, and M. Lenz, "Fiber networks amplify active stress," Proc. Natl. Acad. Sci. U. S. A. 113, 2827–2832 (2016).
- ²⁹ V. Wollrab, J. M. Belmonte, L. Baldauf, M. Leptin, F. Nédeléc, and G. H. Koenderink, "Polarity sorting drives remodeling of actin-myosin networks," J. Cell Sci. 132, jcs219717 (2019).
- ³⁰T. Morris, E. Sue, C. Geniesse, W. M. Brieher, and V. W. Tang, "Synaptopodin stress fiber and contractomere at the epithelial junction," J. Cell Biol. **221**, e202011162 (2022).
- ³¹ J. E. Komianos and G. A. Papoian, "Stochastic ratcheting on a funneled energy landscape is necessary for highly efficient contractility of actomyosin force dipoles," Phys. Rev. X 8, 021006 (2018).
- ³²N. Walani, J. Torres, and A. Agrawal, "Endocytic proteins drive vesicle growth via instability in high membrane tension environment," Proc. Natl. Acad. Sci. U. S. A. 112, E1423–E1432 (2015).
- ³³C. Simon, R. Kusters, V. Caorsi, A. Allard, M. Abou-Ghali, J. Manzi, A. Di Cicco, D. Lévy, M. Lenz, J.-F. Joanny *et al.*, "Actin dynamics drive cell-like membrane deformation," Nat. Phys. **15**, 602–609 (2019).

- ³⁴H. Ni and G. A. Papoian, "Membrane-MEDYAN: Simulating deformable vesicles containing complex cytoskeletal networks," J. Phys. Chem. B **125**, 10710–10719 (2021).
- 35 Y. Tanaka, A. Ishijima, and S. Ishiwata, "Super helix formation of actin filaments in an in vitro motile system," Biochim. Biophys. Acta, Protein Struct. Mol. Enzymol 1159, 94–98 (1992).
- ³⁶N. Leijnse, L. B. Oddershede, and P. M. Bendix, "Helical buckling of actin inside filopodia generates traction," Proc. Natl. Acad. Sci. U. S. A. **112**, 136–141 (2015)
- ³⁷ N. Leijnse, Y. F. Barooji, M. R. Arastoo, S. L. Sønder, B. Verhagen, L. Wullkopf, J. T. Erler, S. Semsey, J. Nylandsted, L. B. Oddershede *et al.*, "Filopodia rotate and coil by actively generating twist in their actin shaft," Nat. Commun. **13**, 1636 (2022).
- ³⁸ A. C. Schramm, G. M. Hocky, G. A. Voth, L. Blanchoin, J.-L. Martiel, and E. M. De La Cruz, "Actin filament strain promotes severing and cofilin dissociation," Biophys. J. **112**, 2624–2633 (2017).
- ³⁹S. K. Vogel, Z. Petrasek, F. Heinemann, and P. Schwille, "Myosin motors fragment and compact membrane-bound actin filaments," Elife **2**, e00116 (2013).
- ⁴⁰S. Deguchi, T. S. Matsui, and M. Sato, "Simultaneous contraction and buckling of stress fibers in individual cells," J. Cell. Biochem. **113**, 824–832 (2012).
- ⁴¹T. Okamoto, T. S. Matsui, T. Ohishi, and S. Deguchi, "Helical structure of actin stress fibers and its possible contribution to inducing their direction-selective disassembly upon cell shortening," Biomech. Model. Mechanobiol. 19, 543–555 (2020).
- ⁴²W. Jung, M. P. Murrell, and T. Kim, "F-actin fragmentation induces distinct mechanisms of stress relaxation in the actin cytoskeleton," ACS Macro Lett. 5, 641–645 (2016).
- ⁴³J. Li, T. Biel, P. Lomada, Q. Yu, and T. Kim, "Buckling-induced F-actin fragmentation modulates the contraction of active cytoskeletal networks," Soft Matter 13, 3213–3220 (2017).
- ⁴⁴ M. P. Murrell and M. L. Gardel, "F-actin buckling coordinates contractility and severing in a biomimetic actomyosin cortex," Proc. Natl. Acad. Sci. U. S. A. 109, 20820–20825 (2012).
- ⁴⁵G. H. Koenderink and E. K. Paluch, "Architecture shapes contractility in actomyosin networks," Curr. Opin. Cell Biol. **50**, 79–85 (2018).
- ⁴⁶ J. M. Ferrer, H. Lee, J. Chen, B. Pelz, F. Nakamura, R. D. Kamm, and M. J. Lang, "Measuring molecular rupture forces between single actin filaments and actin-binding proteins," Proc. Natl. Acad. Sci. U. S. A. 105, 9221–9226 (2008).
- ⁴⁷ M. Rief, R. S. Rock, A. D. Mehta, M. S. Mooseker, R. E. Cheney, and J. A. Spudich, "Myosin-V stepping kinetics: A molecular model for processivity," Proc. Natl. Acad. Sci. U. S. A. 97, 9482–9486 (2000).
- ⁴⁸S. Stuij, J. M. van Doorn, T. Kodger, J. Sprakel, C. Coulais, and P. Schall, "Stochastic buckling of self-assembled colloidal structures," Phys. Rev. Res. 1, 023033 (2019).
- ⁴⁹ M. J. Footer, J. W. J. Kerssemakers, J. A. Theriot, and M. Dogterom, "Direct measurement of force generation by actin filament polymerization using an optical trap," Proc. Natl. Acad. Sci. U. S. A. **104**, 2181–2186 (2007).
- ⁵⁰D. R. Kovar and T. D. Pollard, "Insertional assembly of actin filament barbed ends in association with formins produces piconewton forces," Proc. Natl. Acad. Sci. U. S. A. 101, 14725–14730 (2004).
- ⁵¹S. Forth, C. Deufel, M. Y. Sheinin, B. Daniels, J. P. Sethna, and M. D. Wang, "Abrupt buckling transition observed during the plectoneme formation of individual DNA molecules," Phys. Rev. Lett. 100, 148301 (2008).
- ⁵²F. Rückerl, M. Lenz, T. Betz, J. Manzi, J.-L. Martiel, M. Safouane, R. Paterski-Boujemaa, L. Blanchoin, and C. Sykes, "Adaptive response of actin bundles under mechanical stress," Biophys. J. 113, 1072–1079 (2017).
- ⁵³M. M. A. E. Claessens, M. Bathe, E. Frey, and A. R. Bausch, "Actin-binding proteins sensitively mediate F-actin bundle stiffness," Nat. Mater. 5, 748–753 (2006).
- ⁵⁴K. Lehmann, M. Shayegan, G. A. Blab, and N. R. Forde, "Optical tweezers approaches for probing multiscale protein mechanics and assembly," Front. Mol. Biosci. 7, 577314 (2020).
- ⁵⁵H. Kang, Q. Wen, P. A. Janmey, J. X. Tang, E. Conti, and F. C. MacKintosh, "Nonlinear elasticity of stiff filament networks: Strain stiffening, negative normal

- stress, and filament alignment in fibrin gels," J. Phys. Chem. B 113, 3799–3805 (2009).
- ⁵⁶ M. L. Gardel, J. H. Shin, F. C. MacKintosh, L. Mahadevan, P. A. Matsudaira, and D. A. Weitz, "Scaling of F-actin network rheology to probe single filament elasticity and dynamics," Phys. Rev. Lett. 93, 188102 (2004).
- ⁵⁷ M. L. Gardel, K. E. Kasza, C. P. Brangwynne, J. Liu, and D. A. Weitz, "Chapter 19: Mechanical response of cytoskeletal networks," Methods Cell Biol. **89**, 487–519 (2008).
- ⁵⁸ K. Haase and A. E. Pelling, "Investigating cell mechanics with atomic force microscopy," J. R. Soc., Interface 12, 20140970 (2015).
- ⁵⁹ H. E. Amuasi, C. Heussinger, R. L. C. Vink, and A. Zippelius, "Nonlinear and heterogeneous elasticity of multiply-crosslinked biopolymer networks," New J. Phys. 17, 083035 (2015).
- ⁶⁰ A. P. Liu, D. L. Richmond, L. Maibaum, S. Pronk, P. L. Geissler, and D. A. Fletcher, "Membrane-induced bundling of actin filaments," Nat. Phys. 4, 789–793 (2008).
- ⁶¹T. Litschel and P. Schwille, "Protein reconstitution inside giant unilamellar vesicles," Annu. Rev. Biophys. **50**, 525–548 (2021).
- ⁶²N. Strelnikova, M. Göllner, and T. Pfohl, "Direct observation of alternating stretch-coil and coil-stretch transitions of semiflexible polymers in microstructured flow," Macromol. Chem. Phys. 218, 1600474 (2017).
- ⁶³ V. Kantsler and R. E. Goldstein, "Fluctuations, dynamics, and the stretch-coil transition of single actin filaments in extensional flows," Phys. Rev. Lett. **108**, 038103 (2012).
- ⁶⁴H. Manikantan and D. Saintillan, "Buckling transition of a semiflexible filament in extensional flow," Phys. Rev. E **92**, 041002 (2015).
- ⁶⁵D. Panja, G. T. Barkema, and J. M. J. van Leeuwen, "Dynamics of a double-stranded DNA segment in a shear flow," Phys. Rev. E 93, 042501 (2016).
- ⁶⁶B. Chakrabarti, C. Gaillard, and D. Saintillan, "Trapping, gliding, vaulting: Transport of semiflexible polymers in periodic post arrays," Soft Matter 16, 5534–5544 (2020).
- ⁶⁷R. Chelakkot, R. G. Winkler, and G. Gompper, "Flow-induced helical coiling of semiflexible polymers in structured microchannels," Phys. Rev. Lett. **109**, 178101 (2012).
- ⁶⁸ W. Chen, X. Kong, Q. Wei, H. Chen, J. Liu, and D. Jiang, "Compression and stretching of confined linear and ring polymers by applying force," Polymers 13, 4193 (2021).
- ⁶⁹ K. Ostermeir, K. Alim, and E. Frey, "Buckling of stiff polymer rings in weak spherical confinement," Phys. Rev. E 81, 061802 (2010).
- ⁷⁰H. Wada, "A semiflexible polymer ring acting as a nano-propeller," Eur. Phys. L F 28, 11–16 (2009)
- ⁷¹ P. Cifra and T. Bleha, "Piston compression of semiflexible ring polymers in channels," Macromol. Theory Simul. 30, 2100027 (2021).
- ⁷² J. Kierfeld, K. Baczynski, P. Gutjahr, and R. Lipowsky, "Semiflexible polymers and filaments: From variational problems to fluctuations," AIP Conf. Proc. 1002, 151–185 (2008).
- ⁷³E. Pilyugina, B. Krajina, A. J. Spakowitz, and J. D. Schieber, "Buckling a semiflexible polymer chain under compression," Polymers 9, 99 (2017).
- ⁷⁴ K. Ghamari and A. Najafi, "Buckling instability for a charged and semiflexible polymer," Mod. Phys. Lett. B 25, 2209–2217 (2011).
- ⁷⁵G. M. Cooper, "Structure and organization of actin filaments," in *The Cell: A Molecular Approach* (This is a book published by Sinauer Associates Inc., 2000), Vol. 2.
- ⁷⁶D. Keller, D. Swigon, and C. Bustamante, "Relating single-molecule measurements to thermodynamics," Biophys. J. 84, 733–738 (2003).
- ⁷⁷S. Giordano, "Helmholtz and Gibbs ensembles, thermodynamic limit and bistability in polymer lattice models," Continuum Mech. Thermodyn. 30, 459–483 (2018).
- ⁷⁸F. Manca, S. Giordano, P. L. Palla, R. Zucca, F. Cleri, and L. Colombo, "Elasticity of flexible and semiflexible polymers with extensible bonds in the Gibbs and Helmholtz ensembles," J. Chem. Phys. **136**, 154906 (2012).
- ⁷⁹S. Dutta and P. Benetatos, "Statistical ensemble inequivalence for flexible polymers under confinement in various geometries," Soft Matter **16**, 2114 (2020).

- ⁸⁰L. Blanchoin, R. Boujemaa-Paterski, C. Sykes, and J. Plastino, "Actin dynamics, architecture, and mechanics in cell motility," Physiol. Rev. 94, 235-263 (2014).
- ⁸¹ A. J. Spakowitz and Z.-G. Wang, "Free expansion of elastic filaments," Phys. Rev. E 64, 061802 (2001).
- 82 C. Kurzthaler and T. Franosch, "Bimodal probability density characterizes the elastic behavior of a semiflexible polymer in 2D under compression," Soft Matter 14, 2682-2693 (2018).
- 83 M. Doi, S. F. Edwards, and S. F. Edwards, The Theory of Polymer Dynamics (Oxford University Press, 1988), Vol. 73.
- ⁸⁴J. Samuel and S. Sinha, "Elasticity of semiflexible polymers," Phys. Rev. E **66**, 050801 (2002).
- 85 S. Mehraeen, B. Sudhanshu, E. F. Koslover, and A. J. Spakowitz, "End-to-end distribution for a wormlike chain in arbitrary dimensions," Phys. Rev. E 77, 061803 (2008).
- ⁸⁶J. Kierfeld, K. Baczynski, P. Gutjahr, T. Kühne, and R. Lipowsky, "Modelling semiflexible polymers: Shape analysis, buckling instabilities, and force generation," Soft Matter **6**, 5764–5769 (2010).

 87 Y. Wang and J. Qian, "Buckling of filamentous actin bundles in filopodial
- protrusions," Acta Mech. Sin. 35, 365–375 (2019).

 88 Y. Hayase, T. Sakaue, and H. Nakanishi, "Compressive response and helix for-
- mation of a semiflexible polymer confined in a nanochannel," Phys. Rev. E 95,
- 89 A. A. Evans, S. E. Spagnolie, D. Bartolo, and E. Lauga, "Elastocapillary selffolding: Buckling, wrinkling, and collapse of floating filaments," Soft Matter 9, 1711-1720 (2013).
- ⁹⁰ J. Kierfeld, P. Gutjahr, T. Kühne, P. Kraikivski, and R. Lipowsky, "Buckling, bundling, and pattern formation: From semi-flexible polymers to assemblies of interacting filaments," J. Comput. Theor. Nanosci. 3, 898-911 (2006).
- 91 T. Bleha and P. Cifra, "Force-displacement relations at compression of dsDNA macromolecules," J. Chem. Phys. 151, 014901 (2019).
- ⁹²M. Emanuel, H. Mohrbach, M. Sayar, H. Schiessel, and I. M. Kulić, "Buckling of stiff polymers: Influence of thermal fluctuations," Phys. Rev. E 76, 061907 (2007).
- 93 B. Y. Ha and D. Thirumalai, "A mean-field model for semiflexible chains," J. Chem. Phys. 103, 9408-9412 (1995).
- ⁹⁴B.-Y. Ha and D. Thirumalai, "Semiflexible chains under tension," J. Chem. Phys. 106, 4243-4247 (1997).
- 95 G. Morrison and D. Thirumalai, "Semiflexible chains in confined spaces," Phys. Rev. E 79, 011924 (2009).
- ⁹⁶R. G. Winkler, "Deformation of semiflexible chains," J. Chem. Phys. 118, 2919-2928 (2003).
- 97 J. Tang, X. Zhang, and D. Yan, "Compression induced phase transition of nematic brush: A mean-field theory study," J. Chem. Phys. 143, 204903 (2015).
- ⁹⁸P. L. Hansen, D. Svenšek, V. Adrian Parsegian, and R. Podgornik, "Buckling, fluctuations, and collapse in semiflexible polyelectrolytes," Phys. Rev. E 60, 1956 (1999).

- 99 J. R. Blundell and E. M. Terentjev, "Buckling of semiflexible filaments under compression," Soft Matter 5, 4015-4020 (2009).
- 100 D. Thirumalai and B. Ha, "Statistical mechanics of semiflexible chains: A mean field variational approach," in Theoretical and Mathematical Models in Polymer Research, edited by A. Grosberg (Academic Press, 1998), pp. 15-19.
- ¹⁰¹Y. Teng, N. T. Andersen, and J. Z. Y. Chen, "Statistical properties of a slitconfined wormlike chain of finite length," Macromolecules 54, 8008-8023 (2021).
- 102 A. Marantan and L. Mahadevan, "Mechanics and statistics of the worm-like chain," Am. J. Phys. 86, 86-94 (2018).
- 103 R. Everaers, N. B. Becker, and A. Rosa, "Single-molecule stretching experiments of flexible (wormlike) chain molecules in different ensembles: Theory and a potential application of finite chain length effects to nick-counting in DNA," J. Chem. Phys. 154, 024903 (2021).
- 104 D. R. Tree, A. Muralidhar, P. S. Doyle, and K. D. Dorfman, "Is DNA a good model polymer?," Macromolecules 46, 8369-8382 (2013).
- 105 F. Gittes, B. Mickey, J. Nettleton, and J. Howard, "Flexural rigidity of microtubules and actin filaments measured from thermal fluctuations in shape," J. Cell Biol. 120, 923-934 (1993).
- 106 D. Frenkel and B. Smit, *Understanding Molecular Simulation: From Algorithms* to Applications (Elsevier, 2001), Vol. 1.
- ¹⁰⁷H. Kojima, A. Ishijima, and T. Yanagida, "Direct measurement of stiffness of single actin filaments with and without tropomyosin by in vitro nanomanipulation," Proc. Natl. Acad. Sci. U. S. A. 91, 12962-12966 (1994).
- 108 M. Hinczewski and R. R. Netz, "Anisotropic hydrodynamic mean-field theory for semiflexible polymers under tension," Macromolecules 44, 6972 (2011).
- 109 D. R. Scheff, S. A. Redford, C. Lorpaiboon, S. Majumdar, A. R. Dinner, and M. L. Gardel, "Actin filament alignment causes mechanical hysteresis in cross-linked networks," Soft Matter 17, 5499-5507 (2021).
- 110 D. Zhao, F. Liu, D. L. Huber, and M. G. Lagally, "Step-induced magnetichysteresis anisotropy in ferromagnetic thin films," J. Appl. Phys. 91, 3150-3153
- ¹¹¹P. A. Janmey, M. E. McCormick, S. Rammensee, J. L. Leight, P. C. Georges, and F. C. MacKintosh, "Negative normal stress in semiflexible biopolymer gels," Nat. Mater. 6, 48-51 (2007).
- ¹¹²S. Majumdar, L. C. Foucard, A. J. Levine, and M. L. Gardel, "Mechanical hysteresis in actin networks," Soft Matter 14, 2052-2058 (2018).
- ¹¹³J. Kierfeld, "Force-induced desorption and unzipping of semiflexible polymers," Phys. Rev. Lett. **97**, 058302 (2006).

 114 A. Baumgärtner, "Phase transitions of semiflexible lattice polymers," J. Chem.
- Phys 84, 1905–1908 (1986)
- 115 K. A. Jansen, A. J. Licup, A. Sharma, R. Rens, F. C. MacKintosh, and G. H. Koenderink, "The role of network architecture in collagen mechanics," Biophys. J. 114, 2665-2678 (2018).
- 116 C. Bustamante, Z. Bryant, and S. B. Smith, "Ten years of tension: Singlemolecule DNA mechanics," Nature 421, 423-427 (2003).